
Optimized Dry Cooling for Solar Power Plants

Hansley Narasiah*

University College London

Ouail Kitouni*

Massachusetts Institute of Technology

Andrea Scorsoglio

University of Arizona

Bernd K. Sturdza

Oxford University

Shawn Hatcher

Mississippi State University

Dolores Garcia

CERN

Matt J. Kusner

University College London

Abstract

Concentrated solar power (CSP) plants offer sustainable energy with the benefit of day-to-night energy storage. The recent development of the supercritical carbon dioxide ($s\text{CO}_2$) Brayton cycle made CSP plants cost-competitive. However, the cost of cooling required for these CSP plants can vary wildly depending on design and current cooler designs are far from optimal. Here, we optimize the design and configuration of a dry cooling system. We develop a physics-based simulation of the cooling properties of an air-cooled heat exchanger. Using this simulator, we leverage recent results in high-dimensional Bayesian optimization to find dry cooler designs that minimize lifetime cost, reducing this cost by about 67% compared to recently proposed designs. Our simulation and optimization framework can increase the development pace of economically viable sustainable energy generation systems.

1 Introduction and Background

Concentrated solar power holds promise as a sustainable energy source, in particular, due to the recent reduction in the levelized cost of electricity (LCOE) [11, 15]. However, effective cooling systems remain critical to viability. Supercritical CO_2 ($s\text{CO}_2$) cycles now enable cost-competitive plants [6, 14, 7] contingent on cooling near the CO_2 critical point, making the optimization of air cooler designs crucial. The design of the finned-tube heat exchanger, the core component of the air cooling system, significantly impacts the cost and performance of CSP. This heat exchanger enables heat transfer from the $s\text{CO}_2$ to air and depends on several parameters, such as tube dimensions, fin configurations, and airflow patterns (Figure 7). Although prior efforts to enhance the $s\text{CO}_2$ CSP dry cooler design have primarily focused on individual components like heat exchanger bundles [3], only a few aspects have undergone in-depth examination. This surprising gap in comprehensive investigation suggests that existing dry cooler designs might be more expensive than necessary, signifying the potential for improvement.

We present a method combining simulation and optimization to explore a broad design space. Our physics simulator incorporates thermodynamic principles and empirical correlations to model intricate heat exchanger (HX) configurations. We also implement an expanded cost model accounting for materials, manufacturing, and operation. Finally, we use optimization techniques to find cost-effective designs. Our key insight is a Bayesian optimization strategy exploiting local trust regions to navigate the high-dimensional search space efficiently. This enables comprehensive optimization of air cooler parameters like tube dimensions and fin configurations to minimize total lifetime cost. We demonstrate a 67%+ cost reduction over recent designs, showing the promise of simulation-based

optimization. This framework can accelerate the development of economical renewable energy systems¹.

2 Simulation and Optimization

Overview In this section, an overview of the problem and the approach used to frame it in a general computer science framework is provided. Hence, the notations in this section are unique to this section of the report. The methodological approach is framed around a well-defined optimization goal:

$$\text{minimize } c(\mathbf{x}) \text{ such that } v(\mathbf{x}) = 1 \quad (1)$$

Within this construct, \mathbf{x} represents a design configuration of the dry cooler. The cost function $c(\mathbf{x})$ calculates the cost associated with this design (also referred to as the cost calculator). Meanwhile, $v(\mathbf{x})$ is a binary function designed to assess the viability of the design. When $v(\mathbf{x})$ outputs a value of 1, it implies that the design meets the desired output temperature criteria while preserving the supercritical state of the CO₂ throughout.

At its core, this optimization task is a complex non-linear mixed-integer programming problem, where the design vector \mathbf{x} encapsulates both continuous and integer variables, and both the cost function $c(\mathbf{x})$ and the validity function $v(\mathbf{x})$ have non-linear relationships with \mathbf{x} . Solving such a problem using traditional mixed-integer programming techniques would be computationally daunting and most likely intractable. Instead, a more elegant solution strategy is proposed:

$$\text{minimize } c(p(\mathbf{x})) \quad (2)$$

Here, $p(\mathbf{x})$ refers to a projection function (also referred to as the simulator). Given a design vector \mathbf{x} , it returns a modified design vector \mathbf{x}' such that $v(\mathbf{x}') = 1$. This function ensures that the output design adheres to the critical criteria, namely, achieving the target temperature while maintaining the CO₂ in its supercritical state.

Optimization In our problem setting, the cost function presents significant challenges - it is non-differentiable and relies on external library calls, such as to CoolProp [1], to fetch temperature and pressure data. Since these elements are complex to model directly, traditional gradient-based optimization techniques are unsuitable. The cost of simulator evaluations also needs to make sample efficiency a priority since the simulator evaluations take time, and this time would only increase with more complex and accurate simulators. However, in high-dimensional problems, the space of solutions grows exponentially, making it hard to find the global minima. Alternative optimization methods such as genetic algorithms, finite difference methods, and Bayesian optimization come to mind. Genetic algorithms, while inspired by biological processes, lack solid theoretical guarantees, resulting in unpredictable outcomes. Finite difference methods, albeit reliable, tend to be slow and become inefficient in navigating a high-dimensional problem space.

In contrast, Bayesian optimization, especially when modeled on Gaussian processes (GP), emerges as a promising choice. GPs are well-studied, offering theoretical guarantees. Bayesian optimization strikes a balance between exploration and exploitation, and with the integration of techniques like TurBO [5], it can be strategically applied across the global optimization surface. Leveraging local models ensures a comprehensive and efficient solution to the problem since this makes the framework more scalable [5]. A diagrammatic representation of the optimization process is provided in Figure 1.

Trust Region Bayesian Optimization (TurBO) Bayesian optimization is a probabilistic framework for the optimization of black-box functions. TurBO is a technique that allows scaling to high-dimensional inputs using a collection of local models. This technique retains the rigorous uncertainty estimation of BO and robustness to noisy samples. The core idea behind TurBO is to replace the inefficient and slow convergence of a global model with BO with several independent local surrogate models responsible for much smaller Trust regions (TR) centered around promising solutions. Because of the TR approach, the surrogate models can approximate the objective function much more accurately. TurBO keeps track of m local trust regions each with an independent gaussian process (GP) model. The local posterior \mathcal{GP}^l for $l = \{1, \dots, m\}$, is constrained to TR^l , a hypercube of side L^l . To select the i th candidate across trust regions, a realization from the local posterior in

¹Code: <https://gitlab.com/frontierdevelopmentlab/2022-us-cspcontroller/solair>

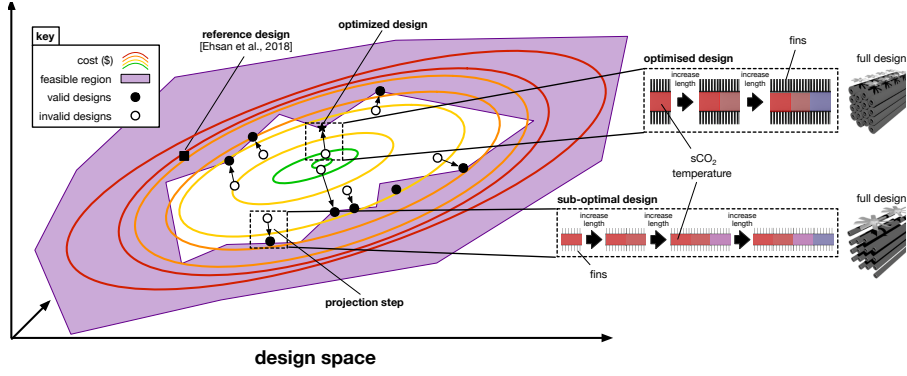


Figure 1: A diagrammatic representation of the optimization process. It shows the design space and illustrates the complexity of the problem by using an optimal design and a sub-optimal one. The cost function is approximated by a Gaussian process and shown as contour curves with red representing higher costs than the green ones. It also illustrates how simply finding the minimum of that surface is insufficient to find the best feasible designs. The projection step is where the simulator operates.

each TR is drawn and the candidate which minimizes the function value across all m samples and trust regions is selected. An optimization run with a list of the parameters optimized are shown in Figure 2 and Table 1 in Appendix A. Note that we use 5 trust regions in the experiments.

Design Cost Accurately modeling the manufacturing and operational costs is crucial for optimization. We implement a cost calculator based on prior work [9, 10, 4] but refine it for this application. The model has three main components: **(1)** Heat exchanger cost: Accounts for materials, labor, overheads, and other factors. **(2)** Fan purchase cost: Initial outlay based on required air flow rates. **(3)** Fan operation cost: Electricity usage over lifetime from power ratings. (see Appendix B for details).

Simulator Implementation The heat exchanger simulator is designed to model and analyze the performance of air-cooled sCO₂ coolers, taking into account various design parameters such as tube dimensions, fin properties, and flow conditions. The implementation employs a combination of energy conservation and empirical correlations to simulate the heat transfer process between CO₂ and air streams.

Several assumptions are made in the simulator to simplify the analysis. These include steady-state operation with constant mass flow rates for both CO₂ and air, constant thermophysical properties within each segment, uniform air distribution across tubes, negligible pressure drop for air, and a segmented approach where tubes are divided into multiple segments treated as individual heat exchanger units. We provide a detailed account of how this was implemented in Appendix D.

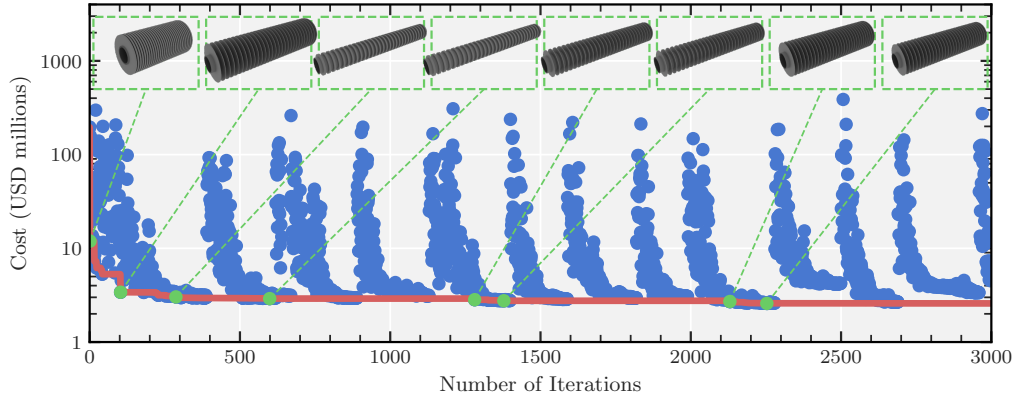


Figure 2: Optimization curve with a rendering of best cost tube designs at selected iterations.

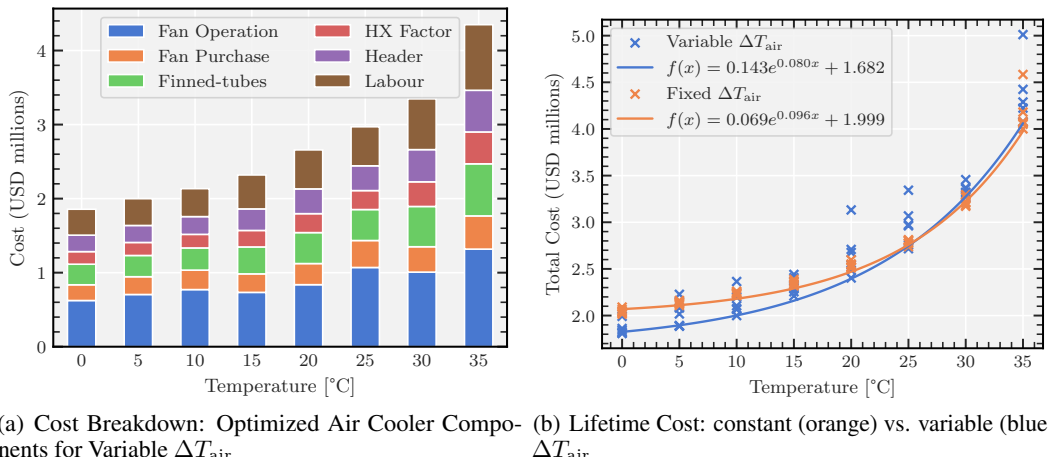
3 Results and Discussion

Single-Run Optimization We show a single optimization run with 3,000 iterations at 20°C ambient temperature. Each blue point is a cost estimate from the full simulation of the cooler using the parameters proposed by TurBO. As seen in the red curve of Figure 2, which represents the minimum cost envelope over iterations, only a few (41) iterations yield improved designs, suggesting inefficiency. The key limitation is the tube length is fixed, not an optimization variable. Still, the figure shows the diversity of designs explored, illustrating the broad search space. Table 1 compares the reference and optimized parameters. Despite limited variables, our approach finds a design with 67% lower lifetime cost. Enabling tube length optimization would improve sample efficiency.

Cost Sensitivity of the Reference and Optimized Design Parameters We assess the cost sensitivity of various design parameters by individually adjusting each to the optimized value obtained through the optimization process while keeping the remaining parameters fixed at their original reference values, with the results depicted in Figure 4. Additionally, we show the differences between the optimized design and the reference value, which indicate significant reductions in the absolute values of the design parameter dimensions, thereby achieving a 67.1% reduction in the lifetime cost (see Table A and Figure 5). Ultimately, a significant amount of savings comes from the changes in design parameters since all the header and labor costs, as well as the HX factor-associated costs, are multiples of the material costs, as described in Appendix B.

Optimized air cooler design at different ambient temperatures The performance of any air cooler is severely affected by ambient air temperature. In a sCO₂ CSP plant, the working fluid has to be cooled down to temperatures close to its critical point at 31°C, our chosen design has a set point of 40.3°C. Cooling down to this temperature becomes increasingly more difficult if the temperature of air approaches the target temperature. To maintain sufficient cooling, either the surface area of heat exchange or the airflow needs to be increased. Both options non-linearly affect the lifetime cost of the air cooler, so finding an ideal solution is, therefore, challenging.

This issue can be addressed with our algorithm, providing an optimized air cooler design for any ambient air temperature. To demonstrate the versatility of the algorithm, we distinguish two scenarios. In the first, simpler scenario, the temperature difference between air in and air out $\Delta T_{\text{air}} = T_{\text{air}_{\text{out}}} - T_{\text{air}_{\text{in}}}$ out is kept constant for all ambient air temperatures. This means that airflow remains constant, and only the surface area of the heat exchanger increases with temperature, limiting the effectiveness of the heat exchanger to predetermined values. In this case, the algorithm optimizes the design of the heat exchanger and calculates the optimized lifetime cost; see orange data in Fig. 3(b).



(a) Cost Breakdown: Optimized Air Cooler Components for Variable ΔT_{air} (b) Lifetime Cost: constant (orange) vs. variable (blue) ΔT_{air}

Figure 3: Optimized air cooler cost for a 25MW CSP plant at varying ambient temperatures.

In the second scenario, we want to include the effectiveness of the heat exchanger in the optimization and thus consider ΔT_{air} as a variable. Now both surface area and air flow are changed simultaneously. Results are given in Fig.3(b)) (blue data) and demonstrate that this more general approach allows a significant additional reduction of the air cooler lifetime cost.

Both datasets exhibit an exponential fit in their minimum costs as temperature varies. The blue dataset has more pronounced deviations from this trend, likely due to its larger optimization parameter space since the ΔT_{air} is allowed to vary in this scenario. This variation in cost can be attributed to local minima encountered within the given runtime of the algorithm. The components of the lifetime costs in the second scenario are shown in Fig.3(a). The results show that both the heat exchanger cost and the cost of the fans increase with temperature. The variations in fan power cost are caused by the algorithm choosing different types of fans at different ambient temperatures.

4 Broader Impact

The development of economical and sustainable energy systems is crucial for addressing climate change and ensuring access to affordable electricity globally. This work demonstrates the promise of physics-based simulation and optimization to accelerate the design of renewable power technologies like concentrated solar power. By reducing air cooling costs, a major expense, the methods presented could enable CSP competitiveness with conventional energy sources. Importantly, the framework is generalizable to optimizing any engineered component, and we encourage its adoption across engineering disciplines. Widespread use of simulation-optimization would enhance design across sectors like aerospace, biomedical, and computing, catalyzing innovation.

Focusing on energy, affordable clean electricity empowers human development through healthcare, education, infrastructure and more. Transitioning to renewables like CSP with integrated sCO₂ thermal storage could reduce competition between nations over rare resources needed for batteries, like lithium and cobalt. Storing energy in sCO₂ instead of batteries that require scarce minerals would alleviate geopolitical tensions. However, scaling new technologies requires thoughtful policies to equitably distribute costs and benefits. Intentional design is also needed to minimize risks like land use impacts. Overall, the simulation tools here represent an opportunity to responsibly shape an energy future that is clean, just and prosperous.

References

- [1] Ian H. Bell, Jorrit Wronski, Sylvain Quoilin, and Vincent Lemort. Pure and Pseudo-pure Fluid Thermophysical Property Evaluation and the Open-Source Thermophysical Property Library CoolProp. *Industrial & Engineering Chemistry Research*, 53(6):2498–2508, 2014. doi: 10.1021/ie4033999. URL <http://pubs.acs.org/doi/abs/10.1021/ie4033999>.
- [2] M Monjurul Ehsan, Xurong Wang, Zhiqiang Guan, and AY Klimenko. Design and performance study of dry cooling system for 25 mw solar power plant operated with supercritical co₂ cycle. *International Journal of Thermal Sciences*, 132:398–410, 2018.
- [3] M Monjurul Ehsan, Sam Duniam, Jishun Li, Zhiqiang Guan, Hal Gurgenci, and Alexander Klimenko. Effect of cooling system design on the performance of the recompression co₂ cycle for concentrated solar power application. *Energy*, 180:480–494, 2019.
- [4] M Monjurul Ehsan, Zhiqiang Guan, Hal Gurgenci, and Alexander Klimenko. Feasibility of dry cooling in supercritical co₂ power cycle in concentrated solar power application: Review and a case study. *Renewable and Sustainable Energy Reviews*, 132:110055, 2020.
- [5] David Eriksson, Michael Pearce, Jacob Gardner, Ryan D Turner, and Matthias Poloczek. Scalable global optimization via local bayesian optimization. *Advances in neural information processing systems*, 32, 2019.
- [6] Pardeep Garg, Pramod Kumar, and Kandadai Srinivasan. Supercritical carbon dioxide brayton cycle for concentrated solar power. *The Journal of Supercritical Fluids*, 76:54–60, 2013.
- [7] Saboora Khatoon and Man-Hoe Kim. Preliminary design and assessment of concentrated solar power plant using supercritical carbon dioxide brayton cycles. *Energy Conversion and Management*, 252:115066, 2022.
- [8] Saboora Khatoon, Shehryar Ishaque, and Man-Hoe Kim. Modeling and analysis of air-cooled heat exchanger integrated with supercritical carbon dioxide recompression brayton cycle. *Energy Conversion and Management*, 232:113895, 2021.
- [9] D.G. Kröger. *Air-cooled Heat Exchangers and Cooling Towers*, volume 1. Penwell Corporation, 2004. ISBN 9780878148967. URL <https://books.google.co.uk/books?id=UmxSAAAAMAAJ>.
- [10] D.G. Kröger. *Air-cooled Heat Exchangers and Cooling Towers*, volume 2. Penwell Corporation, 2004. ISBN 9781593700195. URL <https://books.google.co.uk/books?id=7Efr0q5nL8sC>.
- [11] Francesco La Camera. Renewable power generation costs in 2020–irena. *International Renewable Energy Agency: Masdar City, Abu Dhabi*, 2020.
- [12] S.M. Liao and T. Zhao. Measurements of heat transfer coefficients from supercritical carbon dioxide flowing in horizontal mini/micro channels. *Journal of Heat Transfer-transactions of The Asme - J HEAT TRANSFER*, 124, 06 2002. doi: 10.1115/1.1423906.
- [13] M. Monjurul Ehsan, Zhiqiang Guan, A.Y. Klimenko, and Xurong Wang. Design and comparison of direct and indirect cooling system for 25 MW solar power plant operated with supercritical CO₂ cycle. *Energy Conversion and Management*, 168:611–628, 2018. ISSN 0196-8904. doi: <https://doi.org/10.1016/j.enconman.2018.04.072>. URL <https://www.sciencedirect.com/science/article/pii/S0196890418304205>.
- [14] Ty Neises and Craig Turchi. Supercritical carbon dioxide power cycle design and configuration optimization to minimize levelized cost of energy of molten salt power towers operating at 650 c. *Solar Energy*, 181:27–36, 2019.
- [15] A Palacios, C Barreneche, ME Navarro, and Y Ding. Thermal energy storage technologies for concentrated solar power—a review from a materials perspective. *Renewable Energy*, 156: 1244–1265, 2020.
- [16] W.M. Rohsenow, J.P. Hartnett, and E.N. Ganić. *Handbook of Heat Transfer Applications*, pages 4–237. Mechanical engineering. McGraw-Hill, 1985. ISBN 9780070535534. URL <https://books.google.co.uk/books?id=SJhUAAAAMAAJ>.
- [17] J Saari. Heat Exchanger Thermal Design Guide, Jul 2010.

- [18] Seok Ho Yoon, Ju Hyok Kim, Yun Wook Hwang, Mm Soo Kim, Kyoungdoug Min, and Yongchan Kim. Heat transfer and pressure drop characteristics during the in-tube cooling process of carbon dioxide in the supercritical region. *International Journal of Refrigeration*, 26 (8):857–864, 2003. ISSN 0140-7007. doi: [https://doi.org/10.1016/S0140-7007\(03\)00096-3](https://doi.org/10.1016/S0140-7007(03)00096-3). URL <https://www.sciencedirect.com/science/article/pii/S0140700703000963>.

A Optimized Parameters

Design Parameter	Optimized Value	Reference Value
Tube inner diameter, $d_{\text{tube}}^{\text{in}}$	10.452	20.000
Tube outer diameter, $d_{\text{tube}}^{\text{out}}$	11.497	25.000
Fin inner diameter, $d_{\text{fin}}^{\text{in}}$	11.673	28.000
Fin outer diameter, $d_{\text{fin}}^{\text{out}}$	22.962	57.000
Tube transverse pitch, S_T	37.558	58.000
Fin pitch, s	2.827	2.800
Fin thickness, t_{fin}	0.286	0.500

Table 1: Comparison of parameters for the referenced design and optimized designs. All values are expressed in millimeters.

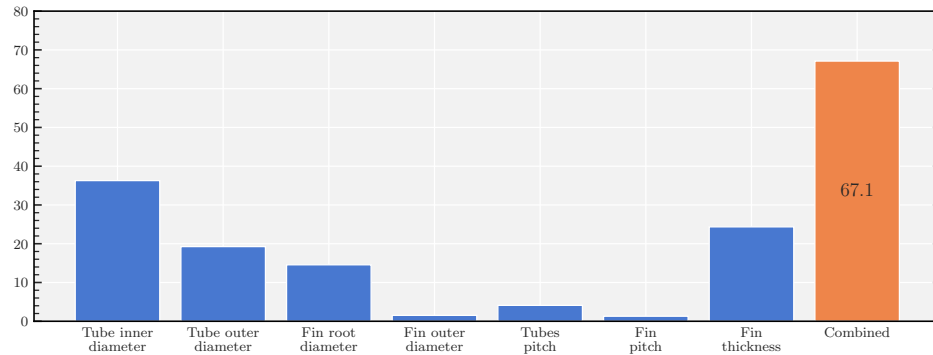


Figure 4: Cost sensitivity of each parameter

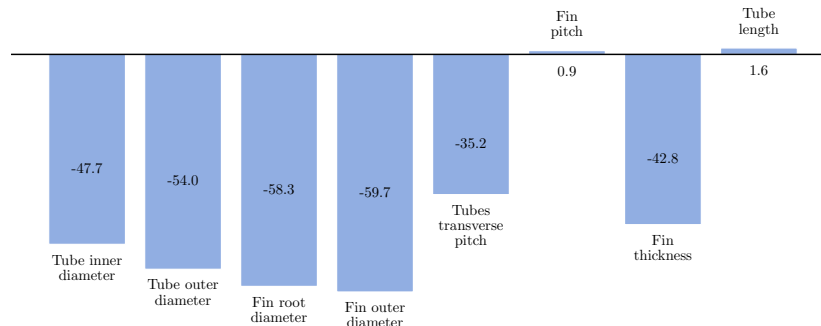


Figure 5: Summary of the differences between the reference and the fully optimized designs as per Table 1

B Cost Calculations

Note the following assumptions in the calculation:

- All parts last an entire lifespan of 25 years.
- Cost of electricity in fan power consumption is assumed to be \$0.05 per kWh.
- No maintenance costs/fouling are considered.
- Fan loading is in an optimal range.
- Forced/induced draft is not considered separately.

The calculation procedure used to calculate the cost of the heat exchanger, that associated with the fan(s), and the resultant total lifetime cost of the heat exchanger, respectively are provided below:

$$L = L_{\text{segment}} \cdot n_{\text{segments}} \quad (3)$$

$$\frac{c_{\text{tube}}}{L} = \frac{\pi (d_{\text{out}}^{\text{tube}} - d_{\text{in}}^{\text{tube}})^2}{4} \rho_{\text{t.m.}} c_{\text{t.m.}} \quad (4)$$

$$\frac{c_{\text{fin}}}{L} = \frac{\pi}{4s} \rho_{\text{f.m.}} c_{\text{f.m.}} \left((d_{\text{out}}^{\text{fin}} - d_{\text{in}}^{\text{fin}})^2 t_{\text{fin}} + (d_{\text{in}}^{\text{fin}} - d_{\text{out}}^{\text{tube}})^2 \cdot (s - t_{\text{fin}}) \right) \quad (5)$$

$$\frac{c_{\text{finned-tube}}}{L} = \left(f_{\text{weighting}} \cdot \left(\frac{c_{\text{tube}}}{L} + \frac{c_{\text{fin}}}{L} \right) \right) + \frac{c_{\text{fixed}}^{\text{finned-tube}}}{L} \quad (6)$$

$$c_{\text{finned-tubes}}^{\text{total}} = \frac{c_{\text{finned-tube}}}{L} \cdot L_{\text{segment}} \cdot n_{\text{segments}} \cdot n_{\text{tubes-in-row}} \cdot n_{\text{rows}} \cdot n_{\text{bundles}} \quad (7)$$

$$c_{\text{air-cooler}}^{\text{no-fans}} = c_{\text{finned-tube}}^{\text{total}} \cdot (1 + f_{\text{header}}) \cdot (1 + f_{\text{labour}}) \cdot f_{\text{HX}} \quad (8)$$

$$c_{\text{fans}}^{\text{initial}} = n_{\text{fans-required}} \cdot c_{\text{fan}}^{\text{purchase}} \quad (9)$$

$$c_{\text{fans}}^{\text{operation}} = n_{\text{fans-required}} \frac{P_{\text{fan}}}{1000} \text{LCOE} (24 \cdot 365 \cdot n_{\text{lifetime-years}}) \quad (10)$$

$$c_{\text{fans}}^{\text{lifetime}} = c_{\text{fans}}^{\text{initial}} + c_{\text{fans}}^{\text{operation}} \quad (11)$$

$$c_{\text{HX}}^{\text{total}} = c_{\text{fans}}^{\text{lifetime}} + c_{\text{air-cooler}}^{\text{no-fans}} \quad (12)$$

where:

- L : total length of the tubes,
- n_{segments} : number of segments comprising the length of tube,
- c_{tube} : cost of tube material in 1 finned-tube,
- $d_{\text{out}}^{\text{tube}}$: outside diameter of tubes,
- $d_{\text{in}}^{\text{tube}}$: inside diameter of tubes,
- $\rho_{\text{t.m.}}$: density of tube material [kg m^{-3}],
- $c_{\text{t.m.}}$: cost of tube material [\$/kg],
- c_{fin} : cost of fin material in 1 finned-tube,
- s : fin pitch, $\rho_{\text{f.m.}}$: density of fin material [kg m^{-3}],
- $c_{\text{f.m.}}$: cost of fin material [\$/kg],
- $d_{\text{out}}^{\text{fin}}$: outside diameter of fins,
- $d_{\text{in}}^{\text{fin}}$: inside diameter of fins,
- t_{fin} : thickness of fins,
- $c_{\text{finned-tube}}$: cost of producing 1 finned-tube,
- $f_{\text{weighting}}$: weighting factor of tube and fin material to estimate total material quantities,
- $c_{\text{finned-tube}}^{\text{fixed}}$: fixed costs associated with producing the finned-tubes,
- $c_{\text{finned-tubes}}^{\text{total}}$: total cost of producing all the finned-tubes in the heat exchanger,
- $n_{\text{tubes-in-row}}$: number of tubes in a row per bundle,
- n_{rows} : number of rows of finned-tubes in the heat exchanger,
- n_{bundles} : number of bundles in the heat exchanger,
- $c_{\text{air-cooler}}^{\text{no-fans}}$: cost of air cooler only (without any fan-associated costs),

- f_{header} : factor applied to calculate the header costs for producing heat exchanger,
- f_{labour} : factor applied to calculate the labour costs in producing the heat exchanger,
- f_{HX} : factor applied on top for entire heat exchanger,
- $c_{\text{fans}}^{\text{initial}}$: cost of purchasing all the fans required to compensate for air pressure drop,
- $n_{\text{fans-required}}$: number of fans required to compensate for air pressure drop,
- $c_{\text{fan}}^{\text{purchase}}$: cost of purchasing 1 fan,
- $c_{\text{fans}}^{\text{operation}}$: cost of operation of fans throughout their lifetime,
- P_{fan} : power requirement of 1 fan [W],
- LCOE: levelized cost of electricity [\$ / kWh],
- $n_{\text{lifetime-years}}$: lifetime of fans in years,
- $c_{\text{fans}}^{\text{lifetime}}$: cost of fans over entire lifetime, and
- $c_{\text{HX}}^{\text{total}}$: total cost of entire heat exchanger over its lifetime.

The total cost comprises the cost of the air cooler itself and the lifetime cost of purchasing and running its fans. The cost of the cooler comprises the material cost of the finned tube (which comprises the cost of the tube and the fins and depends on the length of the tubes, the diameters of tube and fins and fin thickness) weighted to account for overhead related to construction and labour. The lifetime fan cost depends on the number of fans, their power requirement, the levelized cost of electricity, and the predicted lifetime.

C Optimized cooler costs in different regions of the world

We can apply the pipeline we developed for a variety of ambient conditions. While we do not provide a full study of the various costs associated with building CSP plants in different regions around the world, we supply examples of the total expected costs of the cooling systems for a hypothetical power plant in select locations across the globe.

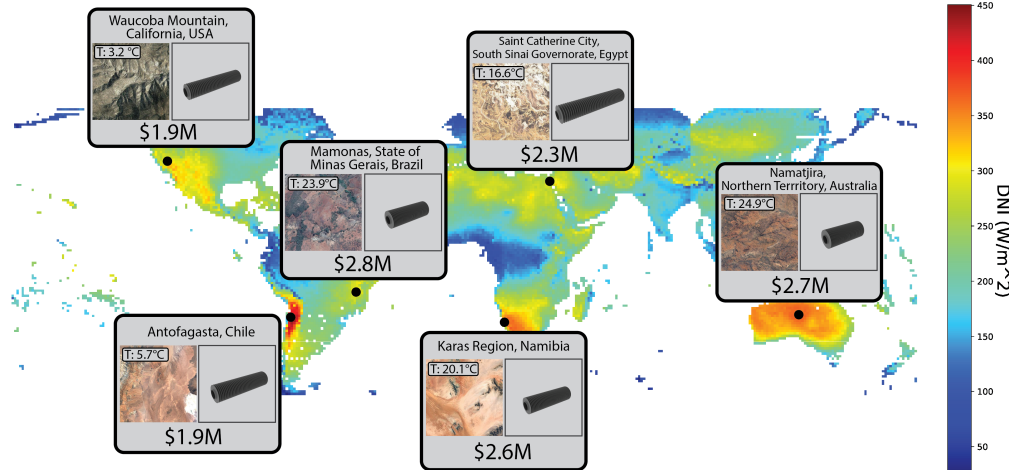


Figure 6: Global mean temperature map and comparison of optimized air cooler cost for a 25 MW CSP plant at selected locations on Earth

D Algorithm

Algorithm 1 1-D sCO₂ Heat-Exchanger Dynamic Length Simulation:

```

Input:  $T_{c(0)}, T_{h(0)}, P_{c(0)}, P_{h(0)}, T_h^{\text{target}}$ 
 $n = 0$ 
while  $T_{h(n)} > T_h^{\text{target}}$  do  $\triangleright$  If final segment temperature is too high increase the # of segments
     $n = n + 1$ 
     $L = T_{h(n-1)} - 1$ 
     $U = T_{h(n-1)}$ 
     $T_{h(n)} = (L + U)/2$ 
     $T_{h(n)} \rightarrow \text{Compute } Q_n, Q_{\text{htc}}$ 
    while  $Q_n \neq Q_{\text{htc}}$  do
         $T_{h(n)} = \text{BinarySearch}(L, U)$ 
         $P_{h(n)} \leftarrow \text{Compute pressure drop}$ 
         $Q_n, Q_{\text{htc}} \leftarrow \text{EnergyBalance}(T_{h(n)}, T_{h(n-1)}, T_{c(0)}, P_{h(n)}, P_{h(n-1)})$ 
    end while
     $Q_{\text{CO2}(n)} \leftarrow \text{HeatReleased}(T_{h(n)}, T_{h(n-1)}, P_{h(n)}, P_{h(n-1)})$ 
     $T_{c(n)} \leftarrow \text{AirTemperature}(Q_{\text{CO2}(n)}, T_{c(0)})$ 
end while

```

We present Algorithm 1 implemented for the heat exchanger dynamic length simulation.

To solve for temperatures and pressures at different points within the system, the simulator employs an iterative approach. First, it initializes a `Simulator` or `DynamicLength` instance with specified design parameters. Then, for each tube row in a sub-heat exchanger, it calls `_solve_tube()` method with initial conditions for CO₂ pressure (`p_co2_init`), temperature (`t_co2_init`), and optionally air inlet temperature(s) (`t_air_init`). This method solves for temperatures and pressures at each segment along a tube by calling `_solve_segment()` method iteratively.

In `_solve_segment()`, binary search is performed on output CO₂ temperature until the energy balance equation is satisfied within specified tolerance limits. For intermediate SHXs after the first one (`_intermediate_shx()`), binary search is performed on initial conditions until mean outlet temperature converges within tolerance limits. The calculated temperatures and pressures for each segment are stored in the results dictionary during the simulation process.

The simulator uses physics-based equations such as energy balance equation to ensure that energy transferred from CO₂ to air through convection equals the energy change in CO₂ due to temperature variation and pressure drop. It also employs Log Mean Temperature Difference (LMTD) to calculate an average temperature difference between hot (CO₂) and cold (air) streams across a segment. Additionally, it computes an Overall Heat Transfer Coefficient based on tube geometry, fluid properties, and flow conditions. Finally, it estimates pressure drop across a segment using Darcy–Weisbach equation or other appropriate correlations.

By combining these physics equations with iterative solution techniques like binary search and segmented approach, this simulator can efficiently solve complex systems like multi-row heat exchangers with varying lengths or designs while maintaining accuracy in performance calculations.

D.1 Simulator

A computational approach to simulate temperature and pressure changes across a direct air-to-CO₂ heat exchanger/dry cooler, specifically in concentrated solar power applications, is replicated as per prior work [8, 2]. This segment-by-segment approach, described in this entire section, allows for detailed adjustments of key design parameters to optimize performance, hence reduce the overall costs of producing and operating such a heat exchanger.

The heat exchanger is first split into two-dimensional segments perpendicular to the cross-section of the tubes. The heat transfer $Q_{i,j}$ in each segment (i, j) is then calculated using:

$$Q_{i,j} = O_{\text{htc}(i,j)} \Delta \bar{T}_{i,j} \quad (13)$$

$$= \dot{m}_c (T_{c(i,j+1)} - T_{c(i,j)}) \quad (14)$$

$$= \dot{m}_h (T_{h(i,j)} - T_{h(i+1,j)}) \quad (15)$$

where \dot{m}_c and \dot{m}_h are the mass flow rates of the air (cold fluid) and the sCO₂ (hot fluid) respectively, and where $\Delta \bar{T}_{i,j}$ is the log-mean temperature difference, defined by:

$$\Delta \bar{T}_{i,j} = \frac{\Delta T_{y_{i,j}} - \Delta T_{x_{i,j}}}{\ln \Delta T_{y_{i,j}} - \ln \Delta T_{x_{i,j}}} \quad (16)$$

with $\Delta T_{y_{i,j}} = T_{h(i,j)} - T_{c(i,j+1)}$ and $\Delta T_{x_{i,j}} = T_{h(i+1,j)} - T_{c(i,j)}$ where T_h and T_c represent the temperatures of the hot and cold fluids respectively.

The overall heat transfer coefficient $O_{\text{htc}(i,j)}$ is then computed as follows:

$$O_{\text{htc}(i,j)} = [R_{t(i,j)} + R_{a(i,j)} + R_{w(i,j)}]^{-1} = \left[\frac{1}{h_s(A_{\text{sCO}_2}^s)} + \frac{1}{h_{\text{air}}(A_{\text{air}}^s)_{\text{eff}}} + 0 \right]_{(i,j)}^{-1} \quad (17)$$

where $R_{t(i,j)}$, $R_{a(i,j)}$, and $R_{w(i,j)}$ are the tube-side, the air-side, and the wall resistances, respectively at segment (i, j) . Note that the wall resistances are assumed to be negligible in the analysis.

The air-side heat transfer cross-sectional and surface areas are given by Equations 18 and 19 respectively [8, 13].

$$A_{\text{air}}^c = (S_T - d_{\text{fin}}^{\text{in}})L_{\text{tube}} - (d_{\text{fin}}^{\text{out}} - d_{\text{fin}}^{\text{in}})t_{\text{fin}}n_{\text{fin}} \quad (18)$$

$$(A_{\text{air}}^s)_{\text{eff}} = \pi d_{\text{fin}}^{\text{in}}(L_{\text{tube}} - t_{\text{fin}}n_{\text{fin}}) + \pi n_{\text{fin}} \left(\frac{d_{\text{fin}}^{\text{out}}{}^2 - d_{\text{fin}}^{\text{in}}{}^2}{2} + d_{\text{fin}}^{\text{out}}t_{\text{fin}} \right) \eta_{\text{fin}} \quad (19)$$

$$A_{\text{sCO}_2}^s = \pi d_{\text{tube}}^{\text{in}}L_{\text{tube}} \quad (20)$$

$$\eta_{\text{fin}} = \frac{\tanh \left(\sqrt{\frac{2h_{\text{air}}}{k_{\text{f.m.}}t_{\text{fin}}}} \Phi \left(\frac{d_{\text{tube}}^{\text{out}}}{2} \right) \right)}{\sqrt{\frac{2h_{\text{air}}}{k_{\text{f.m.}}t_{\text{fin}}}} \Phi \left(\frac{d_{\text{tube}}^{\text{out}}}{2} \right)} \text{ where } \Phi = \left(\frac{d_{\text{fin}}^{\text{out}}}{d_{\text{tube}}^{\text{out}}} - 1 \right) \left[1 + 0.35 \ln \left(\frac{d_{\text{fin}}^{\text{out}}}{d_{\text{tube}}^{\text{out}}} \right) \right] \quad (21)$$

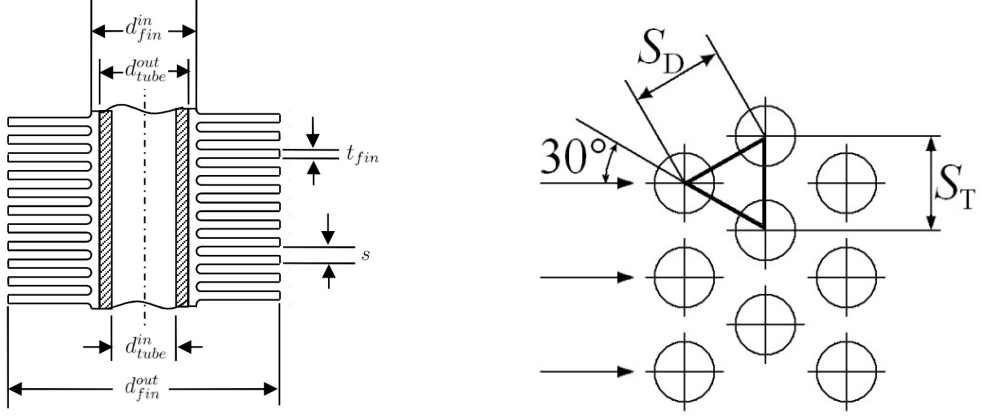
where A_{air}^c : area of cross-section of air exposed to the flow, S_T : transverse pitch of tubes, $d_{\text{fin}}^{\text{in}}$: inside diameter of fins, $d_{\text{fin}}^{\text{out}}$: outside diameter of fins, t_{fin} : thickness of fins, n_{fin} : number of fins on each finned-tube, A_{air}^s : surface area of air exposed to heat exchange, i.e. surface area of tube that is in contact with air, L_{tube} : length of finned-tube, $d_{\text{tube}}^{\text{in}}$: inside diameter of tubes, η_{fin} : fin efficiency, h_{air} : air-side heat transfer coefficient, $d_{\text{tube}}^{\text{out}}$: outside diameter of tubes, $k_{\text{f.m.}}$: thermal conductivity of fin material [$\text{W m}^{-1} \text{K}^{-1}$], and $A_{\text{sCO}_2}^s$: surface area of sCO₂ exposed to heat exchange, surface area of tube that is in contact with sCO₂.

The direct calculation of the outgoing thermodynamic properties in the heat exchanger is complicated due to the complex, non-linear, and non-differentiable factors involved in computing the overall heat transfer coefficient within each segment. Therefore, an iterative approach involving a binary search is used to solve for the outgoing sCO₂ temperature which satisfies Equations 13, 14 and 15. Note that this strategy is based on the assumption that the overall heat transfer coefficient, $O_{\text{htc}(i,j)}$, and by extension the heat transferred, is a monotonic function of outgoing sCO₂ temperature.

It is possible that, for a set of design parameters, a simulation run does not achieve the required outlet sCO₂ properties and to avoid this, the length of the tubes is dynamically adjusted to guarantee a successful design, possibly leading to higher overall cooler volumes and higher material costs. Should the volume be an important design constraint, the current procedure would need to be extended to accommodate this. Note that more detailed descriptions of the simulator are provided later on this section.

Using the same notation for geometrical variables as in Figure 7, the friction coefficients of airflow across finned tubes, $C_{f_{\text{air}}}$ are given below by Equations 22 and 23 for the simplified range of dimensions specified below:

$$C_{f_{\text{air}}} = 9.645 \cdot \text{Re}_{\max}^{-0.316} \left(\frac{S_T}{d_{\text{tube}}^{\text{out}}} \right)^{-0.937} \quad (22)$$



(a) Cross-section of finned-tube showing dimensions [2]

(b) Tube bank with equilateral triangular arrangement:
 $S_T = S_D$ [17]

Figure 7: Finned-tube dimensions and configuration

$$C_{f_{\text{air}}} = 3.805 \cdot \text{Re}_{\max}^{-0.234} \left(\frac{s}{d_{\text{fin}}^{\text{out}}} \right)^{0.251} \left(\frac{s}{L_f} \right)^{-0.759} \left(\frac{d_{\text{fin}}^{\text{out}}}{d_{\text{tube}}^{\text{out}}} \right)^{-0.729} \left(\frac{d_{\text{tube}}^{\text{out}}}{S_T} \right)^{0.709} \left(\frac{S_L}{S_T} \right)^{-0.379} \quad (23)$$

$$L_f = \frac{d_{\text{fin}}^{\text{out}} - d_{\text{fin}}^{\text{in}}}{2} \quad (24)$$

where Re_{\max} : Reynolds number defined with the outside diameter $d_{\text{tube}}^{\text{out}}$ and maximum velocity in the smallest cross-sectional area, and S_L : longitudinal pitch of tube arrangement (in Figure 7(b), using Pythagoras' Theorem: $S_D^2 = S_L^2 + (S_T/2)^2$).

Note that the simplified range of dimensions used, which is a constrained form of the problem, is such that equation 22 is used when the fin size is greater than 0.0063m, and equation 23 is used otherwise. The full set of constraints under which these can be used is provided in prior work [16, 17].

These equations are then used to calculate the air pressure drop across the finned-tube [16, 17]. Note that in this project, the air pressure drop, Δp_{air} is approximated by assuming that four rows of tubes are used with a configuration similar to Figure 7(b) for all designs.

$$\Delta p_{\text{air}} = \frac{G_{\text{air}}^2}{2\rho_{\text{air}}} (C_{f_{\text{air}}} \cdot 4 \cdot n_{\text{rows}}) \quad (25)$$

where G_{air} : flow mass velocity of air [$\text{kg m}^{-2}\text{s}^{-1}$], ρ_{air} : density of air and n_{rows} : number of rows of tube per bundle.

This is then used to calculate the airflow for all the available fans which is in turn used to calculate the number of fans required, n_{fans} as follows:

$$n_{\text{fans}} = \frac{\dot{m}_{\text{air}} \times 3000}{\text{airflow}_{\text{fanmodel}}} \quad (26)$$

where \dot{m}_{air} : mass flow rate of air [kg s^{-1}], the factor of $\times 3000$ is for the conversion of the mass flow rate of air to [$\text{m}^{-3}\text{h}^{-1}$] and $\text{airflow}_{\text{fanmodel}}$: airflow of 1 fan of a specific model [$\text{m}^{-3}\text{h}^{-1}$].

This is then input into the cost calculator as described in Appendix B.

The air-side heat transfer coefficient, h_{air} is given by the following equation [8, 2, 18]:

$$h_{\text{air}} = \frac{k_{\text{air}}}{d_{\text{tube}}^{\text{out}}} \left(0.134 \cdot \text{Pr}_{\text{air}}^{\frac{1}{3}} \text{Re}_{\text{air}}^{0.681} \left(\frac{2(s - t_{\text{fin}})}{d_{\text{fin}}^{\text{out}} - d_{\text{fin}}^{\text{in}}} \right)^{0.2} \left(\frac{s - t_{\text{fin}}}{t_{\text{fin}}} \right)^{0.1134} \right) \quad (27)$$

where Re_{air} : Reynolds number of air, Pr_{air} : Prandtl number of air, k_{air} : thermal conductivity of air [$\text{W m}^{-1} \text{K}^{-1}$], $d_{\text{tube}}^{\text{out}}$: outside diameter of tube, s : fin pitch, t_{fin} : thickness of fins, $d_{\text{fin}}^{\text{out}}$: outside diameter of fin, and $d_{\text{fin}}^{\text{in}}$: inside diameter of fin.

To calculate the heat transfer coefficient of sCO₂, first calculate the pseudo-critical temperature of the fluid at a specified pressure P [bar] using the equation below [8, 12]:

$$T_{pc} = 273.15 - 122.6 + 6.12P - 0.1657P^2 + 0.01773P^{2.5} - 0.0005608P^3 \quad (28)$$

where T_{pc} : pseudo-critical temperature of sCO₂ [K] and P : pressure of sCO₂ [bar].

The sCO₂-side heat transfer coefficient, h_s is then given by the following equation [8, 2, 3, 18]:

$$h_s = \frac{k_s \text{Nu}_s}{d_{\text{tube}}^{\text{in}}} = a (\text{Re}_s)^b (\text{Pr}_s)^c \left(\frac{\rho_{pc}}{\rho_s} \right)^n \left(\frac{k_s}{d_{\text{tube}}^{\text{in}}} \right) \quad (29)$$

$$\text{When } T_s > T_{pc} : a = 0.14, b = 0.69, c = 0.66, n = 0 \quad (29a)$$

$$\text{When } T_s \leq T_{pc} : a = 0.013, b = 1.0, c = -0.05, n = 1.6 \quad (29b)$$

where Re_s : Reynolds number of sCO₂, Pr_s : Prandtl number of sCO₂, Nu_s : Nusselt number of the sCO₂, k_s : thermal conductivity of sCO₂ [W m⁻¹ K⁻¹], ρ_{pc} : density of sCO₂ at pseudo-critical point [kg m⁻³], and ρ_s : density of sCO₂ [kg m⁻³].

The following equations are used to calculate the sCO₂ pressure drop, Δp_s along a tube segment, L_{segment} [8, 2, 18]:

$$C_{f_s} = 8 \left[\left(\frac{8}{\text{Re}_s} \right)^{12} + \left\{ 2.457 \left[\ln \left(\frac{1}{\left(\left(\frac{7}{\text{Re}_s} \right)^{0.9} + 0.27 \left(\frac{\epsilon}{d_{\text{tube}}^{\text{in}}} \right) \right)} \right)^{16} + \left(\frac{37530}{\text{Re}_s} \right)^{16} \right\}^{-\frac{3}{2}} \right]^{1/2} \right] \quad (30)$$

$$u_s = \frac{\dot{m}_s}{\rho_s \frac{\pi (d_{\text{tube}}^{\text{in}})^2}{4}} = \frac{4\dot{m}_s}{\rho_s \pi (d_{\text{tube}}^{\text{in}})^2} \quad (31)$$

$$\Delta p_s = \frac{\rho_s C_{f_s} (u_s)^2}{2d_{\text{tube}}^{\text{in}}} L_{\text{segment}} \quad (32)$$

where ϵ : relative surface roughness of tube, $d_{\text{tube}}^{\text{in}}$: inside diameter of tube, and Re_s : Reynolds number of sCO₂, u_s : flow velocity of sCO₂ [m s⁻¹], ρ_s : density of sCO₂ [kg m⁻³], \dot{m}_s : mass flow rate of sCO₂ [kg s⁻¹], C_{f_s} : friction coefficient of sCO₂ through the tube, and L_{segment} : length of tube segment.

Dynamic Length Simulator The Dynamic Length Simulator (DLS) is designed to optimize the length of tubes in a system by incrementally increasing the number of tube segments until a target temperature is reached. The DLS calculates relevant temperatures along each row, one tube at a time, and employs an energy balance approach to ensure accurate results.

Simulation Process Note that this part of the simulation involves using CoolProp. It is an open-source database of fluid and humid air properties, formulated based on the most accurate formulations in open literature. It has been validated against the most accurate data available from the relevant references [1]. The simulation is described in the following series of steps:

1. Initialisation: The simulation begins by recovering the output air temperature along the length of the previous tube segment
2. Dynamic Scaling: Using dynamically scaled temperature bounds, a binary search over output sCO₂ temperatures is performed for each segment
3. Downstream Propagation: The solver progresses downstream from the first row of tubes that meets a roughly uniform air temperature, and continues downstream for the remaining rows of tubes where each segment encounters monotonically decreasing air temperatures.
4. Energy Balance Propagation: Starting with the inlet sCO₂ temperature, the solver propagates energy balance downstream of the sCO₂ flow along each tube segment. The number of these segments is increased until the average outlet sCO₂ temperature across all tubes (in the first row in contact with the air inlet) reaches the target sCO₂ outlet temperature.

Energy Balance Calculation It is vital that energy conservation is satisfied throughout the simulation process. This is done by calculating the required energy balances in the following steps:

1. Calculate the energy lost by sCO₂ using both guessed output sCO₂ temperature and known input values for air and input sCO₂ temperatures (Equation 15)
2. Determine output air temperature based on energy balance between air and sCO₂ (Equation 14): If air is too hot (hotter than input/output sCO₂), re-evaluate with a higher output sCO₂ temperature.
3. Compute the overall heat transfer (Q_{oht}) from the tube segment at given air and sCO₂ temperatures and pressures using Equation 13. Then:
 - If $Q_{oht} \approx Q_{sCO_2}$: Done
 - If $Q_{oht} > Q_{sCO_2}$: Decrease output sCO₂ temperature due to insufficient heat radiation from sCO₂
 - If $Q_{oht} < Q_{sCO_2}$: Increase output sCO₂ temperature due to excessive heat radiation from CO₂